Higher-order contributions to Rashba and Dresselhaus effects

X. Cartoixà,[1,2,*] L.-W. Wang,[1] D.Z.-Y. Ting,[3] and Y.-C. Chang[4]

[1]*Computational Research Division, Lawrence Berkeley National Laboratory, Berkeley, California 94720, USA*
[2]*Departament d'Enginyeria Electrònica, Universitat Autònoma de Barcelona, 08193 Bellaterra, Barcelona, Spain*
[3]*Jet Propulsion Laboratory, California Institute of Technology, Pasadena, California 91109, USA*
[4]*Department of Physics, University of Illinois at Urbana-Champaign, Urbana, Illinois 61801, USA*

We have developed a method to systematically compute the form of Rashba- and Dresselhaus-like contributions to the spin Hamiltonian of heterostructures to an arbitrary order in the in-plane wave vector $\mathbf{k}_\parallel$. This is achieved by using the double-group representations to construct general symmetry-allowed Hamiltonians with full spin-orbit effects within the tight-binding formalism. We have computed full-zone spin Hamiltonians for [001]-, [110]-, and [111]-grown zinc-blende heterostructures ($D_{2d}, C_{4v}, C_{2v}, C_{3v}$ point-group symmetries), which are commonly used in spintronics. After an expansion of the Hamiltonian up to third order in $\mathbf{k}_\parallel$, we are able to obtain additional terms not found previously. The present method also provides the matrix elements for bulk zinc blendes (T_d) in the anion–cation and effective bond orbital model (EBOM) basis sets with full spin-orbit effects.

I. INTRODUCTION

There has been strong recent interest in spin effects in semiconductors for applications in spintronics.[1,2] In particular, there have been many studies of spin splittings due to bulk inversion asymmetry[3] (BIA), which arises from the different chemical character of the anion and the cation in the zinc-blende structure, and due to structural inversion asymmetry[4] (SIA), which appears at surfaces and interfaces or in layered structures with asymmetric composition or doping, where "top" is different from "bottom." A good understanding of the intraband spin splittings is essential in any attempt to understand the operation of spintronic devices at a microscopic level, since they determine the spin dynamics during relaxation and transport processes.[5–13] The pioneering work by Dresselhaus,[3] Bychkov and Rashba,[4] and D'yakonov and Kachorovskiĭ[6] taught us the functional form of the leading-order contributions—up to first (third) order in the in-plane wave vector $\mathbf{k}_\parallel$ for SIA (BIA)—to the spin Hamiltonians in bulk and heterostructure zinc blendes due to the various sources of inversion asymmetry.

This constructive procedure is of great use as it describes the main physics, but as shown below, $\mathcal{O}(k_\parallel^3)$ contributions for heterostructures due to BIA (Ref. 6) should contain additional terms, while the $\mathcal{O}(k_\parallel^3)$ contributions arising from SIA have not been studied. Thus, it is also important to have a systematic modeling tool which guarantees that all spin-related qualitative features in the band structures will be present. The empirical tight-binding method as formulated by Slater and Koster[14] provides such a systematic way of generating all the symmetry-allowed terms that can appear in a Hamiltonian. It has been used extensively in the computation of bulk, heterostructure, and surface properties, and today finds widespread use in the study of nanostructures involving thousands and even millions of atoms[15] or transport properties.[16]

However, the original formulation by Slater and Koster was obtained through the use of single group-symmetry op-

erations, which prevented it from describing spin effects. Later, Chadi[17] extended the original method with an on-site spin-orbit energy which effectively describes the zone-center split-off splitting and breaks the double degeneracy of the bands for systems without an inversion center. This scheme contains the essential features of spin-orbit interaction, but does not reproduce some qualitative aspects such as the linear spin splitting in valence bands in zinc blendes.[3] Boykin[18] has introduced supplementary matrix elements between nearest-neighbor atomic orbitals as a remedy for zinc-blende structures, but that procedure does not guarantee *a priori* that all spin-orbit effects will be considered and does not treat systematically other types of structures. The development presented in this paper allows us to address these issues precisely.

Experimentally, apart from the large body of indirect observations by Shubnikov–de Haas measurements on semiconductor heterostructures,[19–21] recently there have also been elegant direct photoemission spectroscopy determinations of large SIA-induced (Rashba) spin splittings in two-dimensional electron gases (2DEG's) arising from (111) surface states in metals such as Au, Ag, and Cu, as well as Gd (0001) surfaces.[22–30] While there is at present no conclusive evidence of the importance of these higher-order corrections in experimental situations, 2DEG's with concentrations $\sim 10^{13}$ cm^{-2} have $k_{\parallel,\text{Fermi}} \sim 5\%$ of the Brillouin zone in zinc-blende wells. Higher-order corrections for $k_\parallel$'s at this range should be expected, in a fashion similar to nonparabolicity effects (k^4) in bulk zinc blendes, for which the importance of these effects is well known, particularly in narrow-gap semiconductors. Metal surface 2DEG's, such as in Refs. 24 and 25, or extremely highly phosphorous-doped δ layers[31] have $k_{\parallel,\text{Fermi}}$ that extend even further into the Brillouin zone. Theoretically, nonlinear corrections to the Rashba and Dresselhaus Hamiltonians stemming from numerical diagonalization of large matrices have been shown to have a strong effect on spin lifetimes in quantum wells.[32]

In this article, we compute the forms of SIA and BIA contributions to the spin Hamiltonian of common hetero-

structures, beyond the conventional Rashba[4] and Dresselhaus[3,6] terms, to an arbitrary order in the wave vector $k_\parallel$. This allows us to treat SIA on the same footing as BIA, providing higher-order corrections to the Rashba Hamiltonian for [001] (D_{2d}, C_{4v}, C_{2v}), [110] (C_{2v}, C_s), and [111] (C_{3v}) diamond and zinc-blende quantum wells as well as surface states. We achieve this by following the constructive process of Slater and Koster[14] (SK), but using double-group irreducible representations (irreps) as opposed to single-group irreps. We also apply the method to the generation of bulk zinc-blende (T_d) Hamiltonians in the anion–cation and effective bond orbital model[33,34] (EBOM) basis sets containing full spin-orbit effects. The procedure presented could, of course, also be used for the description of the bands of materials involving heavy elements (i.e., large relativistic effects), such as lead compounds, rare earths, etc.

II. METHODS

In order to achieve our goal of constructing spin Hamiltonians to arbitrary order in the wave vector **k**, we first construct the tight-binding Hamiltonian for the corresponding point-group symmetry using the EBOM basis and then series-expand in **k** to the desired order. Also, since we are interested in the correct description of relativistic and, in particular, spin effects in the electronic bands, we are led naturally to the use of double-group irreps[35] to describe the symmetry operations of the crystal. Thus, if we follow the SK procedure[14] using double as opposed to single groups, we will be assured to obtain the most general Hamiltonian compatible with the crystal symmetries which, by construction, will include all spin-orbit (SO) effects.

Similarly to the invariant expansion of the Hamiltonian (IEH) method by Bir and Pikus,[36] the functional form of the Hamiltonian will be purely determined from symmetry considerations. Both the IEH and the double-group tight-binding (DGTB) method presented here are capable of ultimately producing the same results. But while the IEH inherently provides a perturbative expansion which can involve cumbersome manipulations at high orders, the DGTB can provide a closed form valid for the full Brillouin zone from which the desired perturbation order can be extracted easily. It should be pointed out, however, that small strain effects are more readily obtained with IEH than with DGTB.

The basis states of double-group irreps are much less amenable to brute force algebraic manipulations than their single-group counterparts. Therefore, it becomes necessary to write the tight-binding equations and the symmetry constraints of the parameters in a form that allows computer symbolic manipulation. This is done in Appendixes A and B, yielding the implemented expression for the Hamiltonian matrix element between two Bloch sums:

$$H_{ii'}^{\mu\mu'}(\mathbf{k}) = \sum_{\mathbf{r}_j} \frac{1}{N(\mathbf{r}_j)} \sum_G e^{ik_t D(G)_{tt'}^{\mathrm{vec}} r_{j,t'}} D(G)_{is}^{\mu} E_{ss'}^{\mu\mu'}(\mathbf{r}_j) D(G^{-1})_{s'i'}^{\mu'},$$

(1)

where μ labels an irreducible representation of the point group, i refers to the specific state within an irrep, G is a

point-group operation, and $E_{ss'}^{\mu\mu'}(\mathbf{r}_j)$ is the Hamiltonian matrix element between two states s, s' separated by $\mathbf{r}_j$. The remaining symbols, which are not necessary for the interpretation of the results below, are defined in Appendix A. That appendix, while rederiving the empirical tight-binding basic results, also helps establish a better connection with previous authors' conventions. For our actual double-group calculations we use the irrep matrices $D(G)_{is}^{\mu}$ as provided by Shirai,[37] which correspond to the ones tabulated by Onodera and Okazaki.[38]

III. RESULTS

In order to illustrate the procedure with a familiar example and for comparison purposes, we construct in Sec. III A a four-band model with no spin included for a zinc blende (point group T_d) using an effective bond-orbital basis set. Section III B presents the main results of our work, with spin Hamiltonians for various sorts of quantum wells displaying the terms additional to the Rashba and Dresselhaus Hamiltonians. Finally, we show explicitly in Sec. III C the equivalence between the Löwdin orbitals (LO's) centered at the primitive cell sites [effective bond orbitals (EBO's)] and the zone-center solutions of the $\mathbf{k} \cdot \mathbf{p}$ theory.

The definition of the symbols appearing in the following tables can be found in Eqs. (A4) and (A5) in Appendix A. The phase of the parameters $E_{ij}(\mathbf{r})$—the Hamiltonian matrix elements between a state i at the origin and a state j at **r**—has been factored out in the calculations of the tables. Thus, all $E_{ij}(\mathbf{r})$ are real. Parameters appearing in different tables are, of course, unrelated, while the procedure in Appendix B guarantees a high degree of independence within the parameters in any one table.

A. Single group

We will study the top valence and lowest conduction bands of a zinc blende (point group T_d), which have Γ_5 and Γ_1 symmetry at the zone center [we will use the Koster-Dimmock-Wheeler-Statz (KDWS) notation[39] throughout this paper for the irrep labels (see Fig. 1)]. We consider only coupling to the 12 nearest-neighbor sites. Since we are working with effective bond orbitals located at fcc lattice sites, the nearest neighbors are at $(\frac{1}{2}\frac{1}{2}0)$ and their equivalent positions. Table I shows the matrix elements. The use of the arguments in Appendix B shows, for example, that, with our choice of phases, the whole block $E^{\Gamma_5 \Gamma_5}$ [see Eq. (A5) for meaning] is purely real—which is otherwise trivially obtainable since the Hamiltonian without SO is real and the p orbitals have the same (imaginary) phase—and that $E_{zx}(\frac{1}{2}\frac{1}{2}0) = -E_{xz}(\frac{1}{2}\frac{1}{2}0)$. These results coincide with those of Hass *et al.*,[40] which correct the misprints in Table V of Ref. 14, or those obtained by the different method of adding a d component to p states in an fcc lattice.[41]

B. Double group

In what follows, we present models of quantum wells (QW's) of different symmetries, including structural inver-
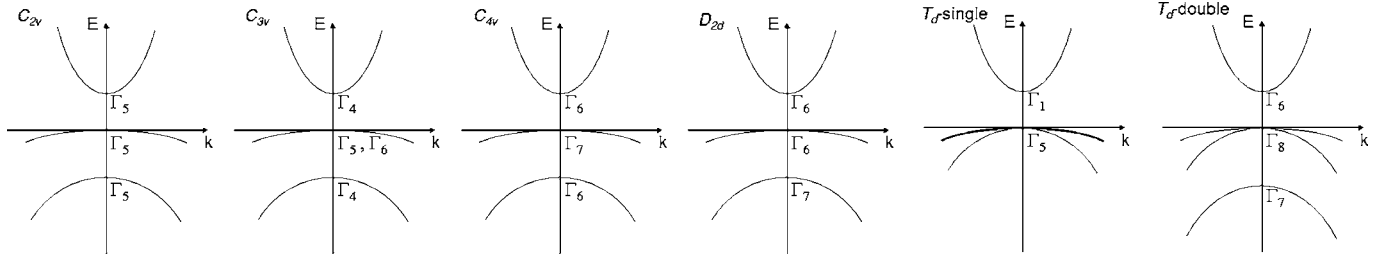
FIG. 1. Labeling of the irreducible representations (irreps) corresponding to the lowest conduction band and the two highest valence bands, at the zone center, for structures with different point group symmetries. Spin splittings at $k \neq 0$ are omitted for clarity.

sion asymmetry[4] effects only, bulk inversion asymmetry[3] only, or both, having in mind the study of in-plane spin transport in two-dimensional electron gases (2DEG's). This has the advantage of yielding less cumbersome expressions than those of the superlattice of the same symmetry, which can be obtained if necessary by setting the matrix elements between supercell instances of different z, $E_{ij}^{\mu\nu}(l,m,n\neq 0)$, to a finite value. Therefore there will be no k_z terms in the Hamiltonian matrix elements. Since these results depend only on the symmetry point group assumed, they can be directly applied to 2DEG realizations other than QW's (e.g., surface states) as long as they have the same underlying symmetry.

Of course, for a numerical zinc-blende nanostructure computation the starting point would be a Hamiltonian derived from the bulk matrix elements given at the end of this section. In this context, the following results should rather be taken as an analytical tool for the study of the bands and the spins and they can be used to test whether calculations from other methods satisfy the symmetry requirements.

1. [001] quantum wells

a. SIA only. In this configuration only the Rashba splitting[4] should appear. These QW's possess C_{4v} symmetry, and an example could be a $Si_{1-x}Ge_x/Si$ QW with an asymmetric Ge concentration profile. For C_{4v} QW's the CB will transform according to Γ_6. We construct a model for the CB

TABLE I. Matrix elements for the zinc-blende structure (single group). The definitions $\xi \equiv k_x a/2$, $\eta \equiv k_y a/2$, and $\zeta \equiv k_z a/2$ are made. The remaining symbols are defined in Eqs. (A4) and (A5). For example, $H_{sx}^{\Gamma_1 \Gamma_5}(\mathbf{k})$ represents the element of the Hamiltonian connecting a state belonging to the Γ_1 irrep with s symmetry to a state belonging to the Γ_5 irrep with x symmetry. The parameters $E_{ij}(\mathbf{r})$ appearing in a table have no relationship with similarly named parameters of a different table.

$H_{ss}^{\Gamma_1 \Gamma_1}(\mathbf{k})$	$E_{ss}(000)$
	$+4E_{ss}(\tfrac{1}{2}\tfrac{1}{2}0)(\cos\xi\cos\eta$
	$+\cos\eta\cos\zeta+\cos\zeta\cos\xi)$
$H_{sx}^{\Gamma_1 \Gamma_5}(\mathbf{k})$	$4iE_{sx}(\tfrac{1}{2}\tfrac{1}{2}0)(\cos\eta+\cos\zeta)\sin\xi-4$
	$E_{sz}(\tfrac{1}{2}\tfrac{1}{2}0)\sin\eta\sin\zeta$
$H_{xx}^{\Gamma_5 \Gamma_5}(\mathbf{k})$	$E_{xx}(000)+4E_{xx}(\tfrac{1}{2}\tfrac{1}{2}0)(\cos\eta+\cos\zeta)\cos\xi$
	$+4E_{zz}(\tfrac{1}{2}\tfrac{1}{2}0)\cos\eta\cos\zeta$
$H_{xy}^{\Gamma_5 \Gamma_5}(\mathbf{k})$	$-4E_{xy}(\tfrac{1}{2}\tfrac{1}{2}0)\sin\xi\sin\eta$
	$+4iE_{xz}(\tfrac{1}{2}\tfrac{1}{2}0)(\cos\xi-\cos\eta)\sin\zeta$

with on-site and second-nearest-neighbor coupling, with the assumption that the supercell instances do not couple to each other, and the results are shown in Table II.

Expanding about the Γ point and keeping terms of up to third order, we obtain

$$
\begin{aligned}
H_{\text{spin}}^{\Gamma_6\Gamma_6} \approx {} & 2a[E_{\uparrow\downarrow}(100)+\sqrt{2}E_{\uparrow\downarrow}(110)](k_y\sigma_x-k_x\sigma_y) \\
& +[E_{\uparrow\downarrow}(100)+\sqrt{2}E_{\uparrow\downarrow}(110)]a^3/3(-k_y^3\sigma_x+k_x^3\sigma_y) \\
& +\sqrt{2}a^3E_{\uparrow\downarrow}(110)k_xk_y(-k_x\sigma_x+k_y\sigma_y).
\end{aligned} \tag{2}
$$

The first term on the right-hand side is, of course, the well-known Rashba Hamiltonian. Here we also derived the two $\mathcal{O}(k_\parallel^3)$ terms, which are the next order in importance. Up to the present there have been calculations that have been carried out to third order in BIA effects but only to linear order in SIA terms.[7] The results from these calculations can be improved and be made consistent within the chosen order of approximation if the higher-order SIA terms are included.

b. BIA only. Here the corresponding point group for a zinc-blende [001] QW is D_{2d}. The different orientation of the bonds at the interfaces [native inversion asymmetry[42] (NIA)] may lower the symmetry to C_{2v}, but this case is equivalent to SIA+BIA and is treated in the next section. Applying Eq. (1) to the CB (Γ_6) we obtain the results in Table III, and expanding close to Γ,

$$
\begin{aligned}
H_{\text{spin}}^{\Gamma_6\Gamma_6} \approx {} & 2a[E_{\uparrow\downarrow}(100)-\sqrt{2}E_{\uparrow\downarrow}(110)](-k_x\sigma_x+k_y\sigma_y) \\
& +\sqrt{2}a^3E_{\uparrow\downarrow}(110)k_xk_y(-k_y\sigma_x+k_x\sigma_y)+[E_{\uparrow\downarrow}(100) \\
& -\sqrt{2}E_{\uparrow\downarrow}(110)]a^3/3(k_x^3\sigma_x-k_y^3\sigma_y).
\end{aligned} \tag{3}
$$

We recover now the Dresselhaus Hamiltonian for [001] zinc-blende quantum wells[6,43,44] in the first two terms. The middle term can be obtained by the procedure of taking the spin Hamiltonian for bulk zinc blendes [Ref. 5 and Eq. (14) below] and substituting k_z^2 for its expectation value in the

TABLE II. Matrix elements for an [001] structure with SIA only described by the C_{4v} point group. The definitions $\xi \equiv k_x a$ and $\eta \equiv k_y a$ are made.

$H_{\uparrow\uparrow}^{\Gamma_6\Gamma_6}$	$E_{\uparrow\uparrow}(000)+2E_{\uparrow\uparrow}(100)(\cos\xi+\cos\eta)$
	$+4E_{\uparrow\uparrow}(110)\cos\xi\cos\eta$
$H_{\uparrow\downarrow}^{\Gamma_6\Gamma_6}$	$2E_{\uparrow\downarrow}(100)(i\sin\xi+\sin\eta)$
	$+2\sqrt{2}E_{\uparrow\downarrow}(110)(i\sin\xi\cos\eta+\cos\xi\sin\eta)$

TABLE III. Same as Table II, but with BIA-only effects (D_{2d}).

$H^{\Gamma_6\Gamma_6}_{\uparrow\uparrow}$	$E_{\uparrow\uparrow}(000)+2E_{\uparrow\uparrow}(100)(\cos\xi+\cos\eta)$
	$\quad+4E_{\uparrow\uparrow}(110)\cos\xi\cos\eta$
$H^{\Gamma_6\Gamma_6}_{\uparrow\downarrow}$	$-2E_{\uparrow\downarrow}(100)(\sin\xi+i\sin\eta)$
	$\quad+2\sqrt{2}E_{\uparrow\downarrow}(110)(\sin\xi\cos\eta+i\cos\xi\sin\eta)$

quantum well.[6] However, the last term cannot be obtained in this fashion,[45] which shows the power of our proposed approach. The symbols $E_{\uparrow\uparrow}(100)$, $E_{\uparrow\downarrow}(110)$, etc., have no relationship with their analogous in the other cases, and the reference to the corresponding point group has been dropped to lighten the notation.

c. SIA+BIA. The corresponding point group for these structures is C_{2v}, and the conduction band is associated with the Γ_5 irrep. Table IV shows the results, and the spin Hamiltonian is

$$H^{\Gamma_5\Gamma_5}_{\text{spin}} \approx -2a\{[E_{\uparrow\downarrow}(010) + 2\,\text{Im}[E_{\uparrow\downarrow}(110)]]k_y\sigma_x + [E_{\uparrow\downarrow}(100)$$
$$+ 2\,\text{Re}[E_{\uparrow\downarrow}(110)]]k_x\sigma_y\} + a^3/3\{[E_{\uparrow\downarrow}(010)$$
$$+ 2\,\text{Im}[E_{\uparrow\downarrow}(110)]]k_y^3\sigma_x + [E_{\uparrow\downarrow}(100)$$
$$+ 2\,\text{Re}[E_{\uparrow\downarrow}(110)]]k_x^3\sigma_y + 6\,\text{Im}[E_{\uparrow\downarrow}(110)]k_x^2k_y\sigma_x$$
$$+ 6\,\text{Re}[E_{\uparrow\downarrow}(110)]k_y^2k_x\sigma_y\}, \tag{4}$$

where Re and Im label real and imaginary parts, respectively.

This Hamiltonian can be transformed into a more familiar form by making the substitutions $E_{\uparrow\downarrow}(010) \to E_{\text{BIA}}+E_{\text{SIA}}$, $E_{\uparrow\downarrow}(100) \to E_{\text{BIA}}-E_{\text{SIA}}$, and $E_{\uparrow\downarrow}(110) \to (E_{\text{BIA},110}+E_{\text{SIA},110})/2+i(E_{\text{BIA},110}-E_{\text{SIA},110})/2$ and reverting to the original axis definitions for the zinc-blende structure:

$$H^{\Gamma_5\Gamma_5}_{\text{spin}} \approx 2a[E_{\text{SIA}} - 2E_{\text{SIA},110}](-k_y\sigma_x + k_x\sigma_y) + 2a[E_{\text{BIA}}$$
$$+ 2E_{\text{BIA},110}](-k_x\sigma_x + k_y\sigma_y) + a^3/6\{[E_{\text{SIA}} - 4E_{\text{SIA},110}]$$
$$\times(k_y^3\sigma_x - k_x^3\sigma_y) + [E_{\text{BIA}} + 4E_{\text{BIA},110}](k_x^3\sigma_x - k_y^3\sigma_y)$$
$$+ 3E_{\text{SIA}}k_xk_y(k_x\sigma_x - k_y\sigma_y) + 3E_{\text{BIA}}k_xk_y(k_y\sigma_x - k_x\sigma_y)\}, \tag{5}$$

which contains the same functional dependence as the sum of the separated SIA- and BIA-only cases, Eqs. (2) and (3).

TABLE IV. Same as Table II, but with SIA and BIA effects (C_{2v}). The phase of $E_{\uparrow\downarrow}(110)$ has not been factored out as it is not determined by symmetry. Thus, Re and Im label its real and imaginary part, respectively.

$H^{\Gamma_5\Gamma_5}_{\uparrow\uparrow}$	$E_{\uparrow\uparrow}(000)+2E_{\uparrow\uparrow}(100)\cos\xi$
	$\quad+2E_{\uparrow\uparrow}(010)\cos\eta+4E_{\uparrow\uparrow}(110)\cos\xi\cos\eta$
$H^{\Gamma_5\Gamma_5}_{\uparrow\downarrow}$	$2E_{\uparrow\downarrow}(100)i\sin\xi-2E_{\uparrow\downarrow}(010)\sin\eta$
	$\quad-4\,\text{Im}[E_{\uparrow\downarrow}(110)]\cos\xi\sin\eta$
	$\quad+4\,\text{Re}[E_{\uparrow\downarrow}(110)]i\sin\xi\cos\eta$
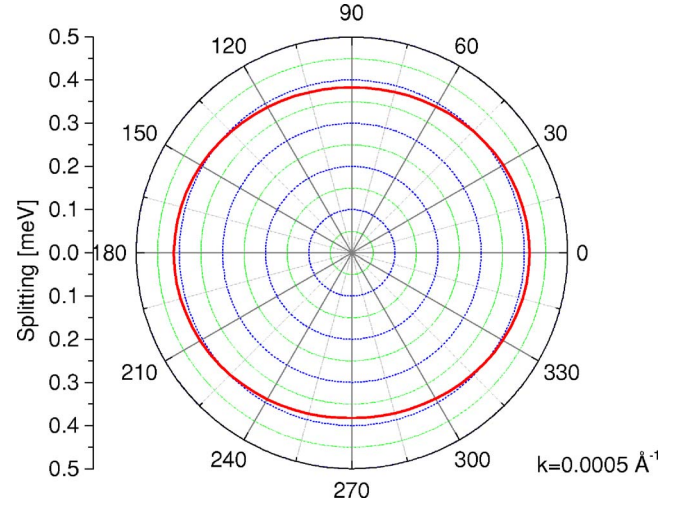
FIG. 2. (Color online) Polar plot of the spin splitting in the CB for a $[110]$ 16/16 AlSb/GaSb/InAs/AlSb QW with SIA only calculated with $\mathbf{k}\cdot\mathbf{p}$. The anisotropy of the splitting is due to the interplay of Rashba- and Dresselhaus-like terms in the spin Hamiltonian, although the simulation only accounts for SIA effects.

2. [110] *quantum wells*

a. SIA only. The symmetry group is C_{2v}, so the results are essentially the same as for $[001]$ heterostructures with BIA +SIA. It is worth noting that, because of the reduced symmetry with respect to SIA-$[001]$, there appear additional Dresselhaus-like terms although for SIA-only one would expect only Rashba terms.

We have verified these predictions with the help of a $\mathbf{k}\cdot\mathbf{p}$ code where BIA effects can be turned on and off[46] for a $[110]$ 16/16 AlSb/GaSb/InAs/AlSb QW (see Fig. 2). We see for this case that the splitting presents a small degree of anisotropy due to the interplay of Rashba- and Dresselhaus-like terms in the spin Hamiltonian, although the simulation only accounts for SIA effects. The axes of constructive and destructive Rashba-Dresselhaus interference are rotated by $\pi/4$ with respect to the $[001]$ BIA+SIA case[44] because here the planes of symmetry coincide with the usual choice of x and y axes, while in the $[001]$ case the reflection planes bisect the x and y axes.

b. BIA only. The symmetry group is again C_{2v}, but now the twofold axis is in-plane, whereas in the previous case it was along the growth direction. This changes the symmetry considerations considerably. The results for a second-nearest-neighbor model are displayed in Table V.

An interesting feature that is recovered is that, for $k_z=0$ (or for a quantum well), the spin will align or antialign along

TABLE V. Matrix elements for an $[110]$ structure with BIA only described by the C_{2v} point group. The definitions $\xi \equiv k_xa_x$ and $\eta \equiv k_ya_y$ are made.

$H^{\Gamma_5\Gamma_5}_{\uparrow\uparrow}$	$E_{\uparrow\uparrow}(000)+2\,\text{Re}[E_{\uparrow\uparrow}(100)]\cos\xi$
	$\quad-2\,\text{Im}[E_{\uparrow\uparrow}(100)]\sin\xi+2E_{\uparrow\uparrow}(010)\cos\eta$
	$\quad+4\,\text{Re}[E_{\uparrow\uparrow}(110)]\cos\xi\cos\eta$
	$\quad-4\,\text{Im}[E_{\uparrow\uparrow}(110)]\sin\xi\cos\eta$
$H^{\Gamma_5\Gamma_5}_{\uparrow\downarrow}$	0

TABLE VI. Matrix elements for a [111] structure described by the C_{3v} point group. The definitions $\xi \equiv k_x a$ and $\eta \equiv k_y a$ are made, and the primitive vectors are taken to be $a(0,1)$ and $a(\sqrt{3}/2, 1/2)$.

$H_{\uparrow\uparrow}^{\Gamma_4\Gamma_4}$	$E_{\uparrow\uparrow}(000)$
	$+2\,\mathrm{Re}[E_{\uparrow\uparrow}(010)](2\cos\sqrt{3}\xi/2\cos\eta/2+\cos\eta)$
	$+2\,\mathrm{Im}[E_{\uparrow\uparrow}(010)](2\cos\sqrt{3}\xi/2\sin\eta/2-\sin\eta)$
	$+2E_{\uparrow\uparrow}(\sqrt{3}00)[\cos\sqrt{3}\xi+\cos(\sqrt{3}\xi/2-3\eta/2)$
	$+\cos(\sqrt{3}\xi/2+3\eta/2)]+$
$H_{\uparrow\downarrow}^{\Gamma_4\Gamma_4}$	$-2E_{\uparrow\downarrow}(010)(\cos\sqrt{3}\xi/2\sin\eta/2+\sin\eta$
	$+i\sqrt{3}\sin\sqrt{3}\xi/2\cos\eta/2)$
	$+iE_{\uparrow\downarrow}(\sqrt{3}00)[2\sin\sqrt{3}\xi+(1$
	$+i\sqrt{3})\sin(\sqrt{3}\xi/2-3\eta/2)$
	$+(1-i\sqrt{3})\sin(\sqrt{3}\xi/2+3\eta/2)]$

the growth direction. This result still holds even when all the neighbors are included: a general $\mathbf{k}_\parallel$ point in the well Brillouin zone has C_s symmetry (reflection with respect to the well plane), which confines the spin to lie perpendicular to the plane. This makes symmetric [110] structures have unusually long spin lifetimes[6,47] for spins along the growth direction because of the suppression of the D'yakonov-Perel' (DP) spin relaxation mechanism.[5] Then, the spin Hamiltonian takes the simple form

$$H_{\mathrm{spin}}^{\Gamma_5\Gamma_5} \approx -2a_x\mathrm{Im}[E_{\uparrow\uparrow}(100)+2E_{\uparrow\uparrow}(110)]k_x\sigma_z$$
$$+ a_x/3\{a_x^2\mathrm{Im}[E_{\uparrow\uparrow}(100)+2E_{\uparrow\uparrow}(110)]k_x^2$$
$$+ a_y^2 6\,\mathrm{Im}[E_{\uparrow\uparrow}(110)]k_y^2\}k_x\sigma_z. \qquad (6)$$

Note that, along the [100] direction, symmetry predicts that the ratio of the $\mathcal{O}(k_x^3)$ splitting coefficient to the $\mathcal{O}(k_x)$ coefficient should be given by $a_x^2/6$, independent of the values of the $E_{ij}(\mathbf{r})$ parameters. This prediction could be verified experimentally, for instance, by using angle-resolved photoemission spectroscopy with sufficient energy resolution.[22,24,25]

c. SIA +BIA. In this case the symmetry will be lowered to C_s (a single reflection plane) and the above arguments will not be able to put any restrictions on the spins. This is further understood if we combine the BIA-only results, which keep the spins pointing along the growth direction, with the SIA-only results, which tend to keep the spins perpendicular to the growth axis. Thus, the spins will point in a general direction dependent on the particular structure under study.

3. [111] *quantum wells*

For BIA-only, these quantum wells transform according to the C_{3v} point group,[48] which consists of the identity, two threefold rotations about the growth axis, and three reflection planes separated by 120° that contain the threefold axis. It is easy to see by inspection that the inclusion of SIA does not reduce the symmetry with respect to the BIA-only case. Thus, here it is only necessary to derive the TB Hamiltonian for C_{3v} structures, which is shown in Table VI.

The expansion about the Γ point yields a spin Hamiltonian

$$H_{\mathrm{spin}}^{\Gamma_4\Gamma_4} \approx 3a[\sqrt{3}E_{\uparrow\downarrow}(\sqrt{3}00)-E_{\uparrow\downarrow}(010)](k_y\sigma_x-k_x\sigma_y)$$
$$+ a^3/8\{[3E_{\uparrow\downarrow}(010)-9\sqrt{3}E_{\uparrow\downarrow}(\sqrt{3}00)]k^2(k_y\sigma_x-k_x\sigma_y)$$
$$+ 2\,\mathrm{Im}[E_{\uparrow\uparrow}(010)](-3k_x^2+k_y^2)k_y\sigma_z\}. \qquad (7)$$

Thus, no matter the situation in [111] QW's, we only have—at $\mathcal{O}(k_\parallel)$—Rashba-like terms, as shown previously with a different method.[13] This is important because the Rashba contribution can be tuned through the action of a gate bias and it is in principle possible to make the first-order spin splitting vanish, suppressing the DP spin relaxation mechanism for all components at the same time.[13]

4. *Zinc blendes with effective bond orbitals*

Here we will construct the model equivalent to the $H^{\Gamma_5\Gamma_5}$ block in Sec. III A, but with spin. Thus, it will include a heavy- and light-hole Γ_8 and a split-off Γ_7 set of states. We provide the symmetry-constrained matrices $E^{\Gamma_i\Gamma_j}$, as they are the primary quantities in nanostructures:

$$E^{\Gamma_8\Gamma_8}\left(\tfrac{1}{2}\tfrac{1}{2}0\right) = \begin{pmatrix} E_{33} & \omega^*E_{31} & iE_{3\bar{1}} & \omega E_{3\bar{3}} \\ -\omega E_{31} & E_{11} & \omega^*E_{1\bar{1}} & iE_{3\bar{1}} \\ -iE_{3\bar{1}} & -\omega E_{1\bar{1}} & E_{11} & \omega^*E_{31} \\ -\omega^*E_{3\bar{3}} & -iE_{3\bar{1}} & -\omega E_{31} & E_{33} \end{pmatrix}, \qquad (8)$$

$$E^{\Gamma_8\Gamma_7}\left(\tfrac{1}{2}\tfrac{1}{2}0\right) = \begin{pmatrix} \omega^*E_{3\uparrow} & iE_{\bar{3}\uparrow} \\ E_{1\uparrow} & \omega^*E_{\bar{1}\uparrow} \\ \omega E_{\bar{1}\uparrow} & -E_{1\uparrow} \\ iE_{3\uparrow} & \omega E_{3\uparrow} \end{pmatrix}, \qquad (9)$$

$$E^{\Gamma_7\Gamma_8}\left(\tfrac{1}{2}\tfrac{1}{2}0\right) = \begin{pmatrix} -\omega E_{3\uparrow} & E_{1\uparrow} & -\omega^*E_{\bar{1}\uparrow} & -iE_{\bar{3}\uparrow} \\ -iE_{3\uparrow} & -\omega E_{\bar{1}\uparrow} & E_{1\uparrow} & -\omega^*E_{3\uparrow} \end{pmatrix}, \qquad (10)$$

and

$$E^{\Gamma_7\Gamma_7}\left(\tfrac{1}{2}\tfrac{1}{2}0\right) = \begin{pmatrix} E_{\uparrow\uparrow} & \omega^*E_{\uparrow\downarrow} \\ -\omega E_{\uparrow\downarrow} & E_{\uparrow\uparrow} \end{pmatrix}, \qquad (11)$$

where $\omega \equiv e^{i\pi/4}$, $\bar{l} \equiv -l$, l refers to $|\phi_{l/2}^{\Gamma_8}\rangle$ and $\uparrow$ ($\downarrow$) refers to $|\phi_{1/2}^{\Gamma_7}\rangle$ ($|\phi_{-1/2}^{\Gamma_7}\rangle$), and the phase factors are explicitly shown so that all parameters E_{ij} are real. Thus, using symmetry operations, the 36 initial matrix elements are reduced to 12 independent parameters. The matrix elements $E^{\Gamma_i\Gamma_j}(G\mathbf{r}_j)$ for the remaining nearest-neighbor sites are obtained combining Eqs. (8)–(11) and (A8).

Now we can construct the bulk tight-binding matrix elements, which will be the foundation for further analysis of the meaning of the parameters. Table VII shows the computed matrix elements from Eqs. (1) and (B8). The remaining matrix elements can be obtained from the Hermiticity of

TABLE VII. Matrix elements for the zinc-blende structure (double group). The remaining matrix elements can be obtained from the hermiticity of the Hamiltonian in the Bloch sum representation. The definitions $\xi \equiv k_x a/2$, $\eta \equiv k_y a/2$, $\zeta \equiv k_z a/2$, are made.

$H_{33}^{\Gamma_8 \Gamma_8}(\mathbf{k})$	$E_{33}(000) + [3E_{11}(\frac{1}{2}\frac{1}{2}0) + E_{3\bar{3}}(\frac{1}{2}\frac{1}{2}0)](\cos\xi\cos\eta + \cos\eta\cos\zeta + \cos\zeta\cos\xi) + 3E_{33}(\frac{1}{2}\frac{1}{2}0)\cos\xi\cos\eta$
	$+\frac{1}{2}[3E_{1\bar{1}}(\frac{1}{2}\frac{1}{2}0) + 2\sqrt{3}E_{31}(\frac{1}{2}\frac{1}{2}0) - E_{3\bar{3}}(\frac{1}{2}\frac{1}{2}0)](\cos\xi - \cos\eta)\sin\zeta$
$H_{11}^{\Gamma_8 \Gamma_8}(\mathbf{k})$	$E_{33}(000) + [3E_{33}(\frac{1}{2}\frac{1}{2}0) + E_{11}(\frac{1}{2}\frac{1}{2}0)](\cos\xi\cos\eta + \cos\eta\cos\zeta + \cos\zeta\cos\xi) + 3E_{11}(\frac{1}{2}\frac{1}{2}0)\cos\xi\cos\eta$
	$-\frac{1}{2}[E_{1\bar{1}}(\frac{1}{2}\frac{1}{2}0) - 2\sqrt{3}E_{31}(\frac{1}{2}\frac{1}{2}0) - 3E_{3\bar{3}}(\frac{1}{2}\frac{1}{2}0)](\cos\xi - \cos\eta)\sin\zeta$
$H_{31}^{\Gamma_8 \Gamma_8}(\mathbf{k})$	$-[\sqrt{2}E_{31}(\frac{1}{2}\frac{1}{2}0) + \sqrt{3/2}(E_{1\bar{1}}(\frac{1}{2}\frac{1}{2}0) + E_{3\bar{3}}(\frac{1}{2}\frac{1}{2}0))](\sin\xi + i\sin\eta)\cos\zeta + 2\sqrt{2}E_{31}(\frac{1}{2}\frac{1}{2}0)(\sin\xi\cos\eta + i\cos\xi\sin\eta)$
	$+4E_{3\bar{1}}(\frac{1}{2}\frac{1}{2}0)(\sin\xi - i\sin\eta)\sin\zeta$
$H_{3\bar{1}}^{\Gamma_8 \Gamma_8}(\mathbf{k})$	$[-\sqrt{2}E_{31}(\frac{1}{2}\frac{1}{2}0) + \sqrt{3/2}(E_{1\bar{1}}(\frac{1}{2}\frac{1}{2}0) + E_{3\bar{3}}(\frac{1}{2}\frac{1}{2}0))](\cos\xi + \cos\eta)\sin\zeta + \sqrt{3}(E_{11}(\frac{1}{2}\frac{1}{2}0)$
	$- E_{33}(\frac{1}{2}\frac{1}{2}0))(\cos\xi - \cos\eta)\cos\zeta - 4iE_{3\bar{1}}(\frac{1}{2}\frac{1}{2}0)\sin\xi\sin\eta$
$H_{3\bar{3}}^{\Gamma_8 \Gamma_8}(\mathbf{k})$	$[-3E_{1\bar{1}}(\frac{1}{2}\frac{1}{2}0)/\sqrt{2} + \sqrt{6}E_{31}(\frac{1}{2}\frac{1}{2}0) + E_{3\bar{3}}(\frac{1}{2}\frac{1}{2}0)/\sqrt{2}](\sin\xi - i\sin\eta)\cos\zeta + 2\sqrt{2}E_{3\bar{3}}(\frac{1}{2}\frac{1}{2}0)(-\sin\xi\cos\eta + i\cos\xi\sin\eta)$
$H_{1\bar{1}}^{\Gamma_8 \Gamma_8}(\mathbf{k})$	$-[E_{1\bar{1}}(\frac{1}{2}\frac{1}{2}0)/\sqrt{2} + \sqrt{6}E_{31}(\frac{1}{2}\frac{1}{2}0) - 3E_{3\bar{3}}(\frac{1}{2}\frac{1}{2}0)/\sqrt{2}](\sin\xi + i\sin\eta)\cos\zeta + 2\sqrt{2}E_{1\bar{1}}(\frac{1}{2}\frac{1}{2}0)(\sin\xi\cos\eta + i\cos\xi\sin\eta)$
$H_{\bar{3}\bar{3}}^{\Gamma_8 \Gamma_8}(k_x,k_y,k_z) = H_{33}^{\Gamma_8 \Gamma_8}(k_x,-k_y,-k_z)$;	$H_{\bar{1}\bar{1}}^{\Gamma_8 \Gamma_8}(k_x,k_y,k_z) = H_{11}^{\Gamma_8 \Gamma_8}(k_x,-k_y,-k_z)$
$H_{\bar{1}\bar{3}}^{\Gamma_8 \Gamma_8}(k_x,k_y,k_z) = H_{31}^{\Gamma_8 \Gamma_8 *}(k_x,-k_y,-k_z)$;	$H_{13}^{\Gamma_8 \Gamma_8}(k_x,k_y,k_z) = H_{31}^{\Gamma_8 \Gamma_8 *}(k_x,-k_y,-k_z)$
$H_{\uparrow\uparrow}^{\Gamma_7 \Gamma_7}(\mathbf{k})$	$E_{\uparrow\uparrow}(000) + 4E_{\uparrow\uparrow}(\frac{1}{2}\frac{1}{2}0)(\cos\xi\cos\eta + \cos\eta\cos\zeta + \cos\zeta\cos\xi) + 2\sqrt{2}E_{\uparrow\downarrow}(\frac{1}{2}\frac{1}{2}0)(\cos\xi - \cos\eta)\sin\zeta$
$H_{\uparrow\downarrow}^{\Gamma_7 \Gamma_7}(\mathbf{k})$	$2\sqrt{2}E_{\uparrow\downarrow}(\frac{1}{2}\frac{1}{2}0)[(\cos\eta - \cos\zeta)\sin\xi - i(\cos\zeta - \cos\xi)\sin\eta]$
$H_{\downarrow\downarrow}^{\Gamma_7 \Gamma_7}(k_x,k_y,k_z) = H_{\uparrow\uparrow}^{\Gamma_7 \Gamma_7}(k_x,-k_y,-k_z)$	
$H_{3\uparrow}^{\Gamma_8 \Gamma_7}(\mathbf{k})$	$2\sqrt{2}E_{3\uparrow}(\frac{1}{2}\frac{1}{2}0)(\sin\xi\cos\eta + i\cos\xi\sin\eta) - (\sqrt{2}E_{3\uparrow}(\frac{1}{2}\frac{1}{2}0) + \sqrt{6}E_{\bar{1}\uparrow}(\frac{1}{2}\frac{1}{2}0))(\sin\xi + i\sin\eta)\cos\zeta$
	$+2E_{\bar{3}\uparrow}(\frac{1}{2}\frac{1}{2}0)(\sin\xi - i\sin\eta)\sin\zeta$
$H_{1\uparrow}^{\Gamma_8 \Gamma_7}(\mathbf{k})$	$4E_{1\uparrow}(\frac{1}{2}\frac{1}{2}0)\cos\xi\cos\eta - 2E_{1\uparrow}(\frac{1}{2}\frac{1}{2}0)(\cos\xi + \cos\eta)\cos\zeta - (\sqrt{6}E_{3\uparrow}(\frac{1}{2}\frac{1}{2}0) + \sqrt{2}E_{\bar{1}\uparrow}(\frac{1}{2}\frac{1}{2}0))(\cos\xi - \cos\eta)\sin\zeta$
$H_{\bar{1}\uparrow}^{\Gamma_8 \Gamma_7}(\mathbf{k})$	$2\sqrt{2}E_{\bar{1}\uparrow}(\frac{1}{2}\frac{1}{2}0)(-\sin\xi\cos\eta + i\cos\xi\sin\eta) + (\sqrt{6}E_{3\uparrow}(\frac{1}{2}\frac{1}{2}0) - \sqrt{2}E_{\bar{1}\uparrow}(\frac{1}{2}\frac{1}{2}0))(\sin\xi - i\sin\eta)\cos\zeta$
	$+2\sqrt{3}E_{\bar{3}\uparrow}(\frac{1}{2}\frac{1}{2}0)(\sin\xi + i\sin\eta)\sin\zeta$
$H_{\bar{3}\uparrow}^{\Gamma_8 \Gamma_7}(\mathbf{k})$	$-4iE_{\bar{3}\uparrow}(\frac{1}{2}\frac{1}{2}0)\sin\xi\sin\eta - 2\sqrt{3}E_{1\uparrow}(\frac{1}{2}\frac{1}{2}0)(\cos\xi - \cos\eta)\cos\zeta + (\sqrt{2}E_{3\uparrow}(\frac{1}{2}\frac{1}{2}0) - \sqrt{6}E_{\bar{1}\uparrow}(\frac{1}{2}\frac{1}{2}0))(\cos\xi + \cos\eta)\sin\zeta$
$H_{\bar{3}\downarrow}^{\Gamma_8 \Gamma_7}(k_x,k_y,k_z) = -H_{3\uparrow}^{\Gamma_8 \Gamma_7}(k_x,-k_y,-k_z)$;	$H_{\bar{1}\downarrow}^{\Gamma_8 \Gamma_7}(k_x,k_y,k_z) = -H_{1\uparrow}^{\Gamma_8 \Gamma_7}(k_x,-k_y,-k_z)$;
$H_{1\downarrow}^{\Gamma_8 \Gamma_7}(k_x,k_y,k_z) = -H_{\bar{1}\uparrow}^{\Gamma_8 \Gamma_7}(k_x,-k_y,-k_z)$;	$H_{3\downarrow}^{\Gamma_8 \Gamma_7}(k_x,k_y,k_z) = -H_{\bar{3}\uparrow}^{\Gamma_8 \Gamma_7}(k_x,-k_y,-k_z)$;

the Hamiltonian in the Bloch sum representation. We can obtain information about the physical effects that are included in this model by expanding the matrix elements about the Γ point[33] and comparing to $\mathbf{k \cdot p}$ results.[49] Similar expansions to obtain $\mathbf{k \cdot p}$ parameters from atomic-orbital-based tight-binding Hamiltonians have also been made by Jancu *et al.*[50]

We focus first on the heavy-hole (HH) and light-hole (LH) bands, given by the Γ_7 irrep. Empirical tight-binding (ETB) implementations based on atomic or bond orbitals with the addition of on-site spin-orbit[17,41] yield an incorrect intraband splitting proportional to k^3 along [110], while Dresselhaus showed[3] from symmetry arguments that it should be linear with k. Our current method solves this problem. From $\mathbf{k \cdot p}$ theory we know that a parameter C describes the linear splitting.[49] Looking, for example, at the $H_{33}^{\Gamma_8 \Gamma_8}$ matrix element and comparing to the corresponding $\mathbf{k \cdot p}$ matrix element $-\sqrt{3}C(k_x + ik_y)/2$, we can identify

$$C = \sqrt{2}a\left[\sqrt{3}E_{1\bar{1}}\left(\tfrac{1}{2}\tfrac{1}{2}0\right) - 2E_{31}\left(\tfrac{1}{2}\tfrac{1}{2}0\right) + \sqrt{3}E_{3\bar{3}}\left(\tfrac{1}{2}\tfrac{1}{2}0\right)\right].$$

(12)

If the parameters in C were calculated from single-group theory, we would obtain $E_{1\bar{1}}(\frac{1}{2}\frac{1}{2}0) = -2\sqrt{2}E_{xz}(\frac{1}{2}\frac{1}{2}0)/3$, $E_{31}(\frac{1}{2}\frac{1}{2}0) = -\sqrt{2/3}E_{xz}(\frac{1}{2}\frac{1}{2}0)$, and $E_{3\bar{3}}(\frac{1}{2}\frac{1}{2}0) = 0$, yielding $C = 0$ and, therefore, no linear splitting in the HH-LH bands.

Figure 3 shows the calculated HH, LH, and SO bands for bulk GaSb. For actual calculations to show the inclusion of the effect, we set the double-group parameters to the single-group values as determined from the EBOM method,[33] with the addition of $E_{3\bar{3}}(\frac{1}{2}\frac{1}{2}0) = \sqrt{2/3}C/a$. We have taken $C = 0.7$ meV Å as calculated by Cardona *et al.*[51] Plot (a) shows the full zone bands. The inclusion of $E_{3\bar{3}}(\frac{1}{2}\frac{1}{2}0)$ makes no appreciable change to the bands at the scale of the plot (i.e., no linear splitting is visible at this scale). Plot (b) is a closer look at the HH and LH bands at the top of the valence band comparing the method presented here (solid lines) and a previous EBOM implementation allowing for bulk inversion asymmetry[41] (dashed lines). Only the present method reproduces the linear splittings, in accordance with the predictions from group theory,[3] showing that the linear splitting arises from off-site SO interactions, which were not included in Ref. 41. In this particular case, the scale of the energy is tiny and it makes little sense to make any claim when such small energy scales are involved. Nevertheless, this example shows that it is indeed possible to describe correctly *all* spin-orbit effects within a tight-binding framework and, moreover, the effects of a finite C have been observed experimentally for GaSb in hole transport measurements.[52,53]

We now turn our attention to the lowest conduction band in zinc blendes, which is associated with the Γ_6 irrep. All the symmetry-equivalent points of $(\frac{1}{2}\frac{1}{2}0)$ are spanned by the proper rotations of T_d, which under Γ_6 correspond to the
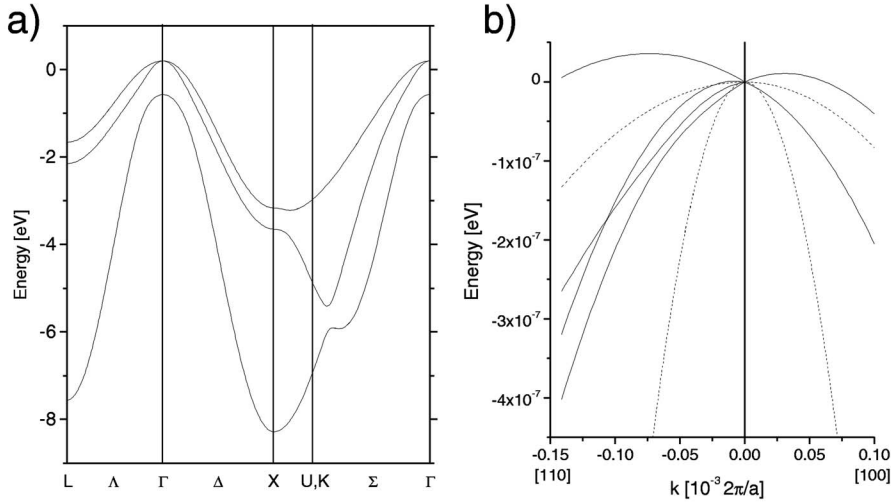
FIG. 3. (a) Full-zone HH, LH, and SO bands for GaSb. (b) Bands very close to the zone center along [100] and [110] directions calculated with the present method (solid lines), featuring the linear splitting and calculated with the method of Ref. 41 (dashed lines).

same matrices as Γ_7. Therefore, the $H^{\Gamma_7\Gamma_7}$ matrix elements remain unchanged under the substitution $\Gamma_7 \rightarrow \Gamma_6$, leading to a full-zone spin Hamiltonian

$$H_{\text{spin}}^{\Gamma_6\Gamma_6} = 2\sqrt{2}E_{\uparrow\downarrow}^{\Gamma_6\Gamma_6}\left(\tfrac{1}{2}\tfrac{1}{2}0\right)[\sigma_z(\cos\xi - \cos\eta)\sin\zeta + \text{c.p.}], \tag{13}$$

where "c.p." stands for cyclic permutations and which, after expanding to lowest order about the zone center, allows us to recover the k^3 Hamiltonian[5]

$$H_{\text{spin}}^{\Gamma_6\Gamma_6} \approx \gamma_c[(k_x^2 - k_y^2)k_z\sigma_z + \text{c.p.}], \tag{14}$$

with $\gamma_c \equiv a^3/(2\sqrt{2})E_{\uparrow\downarrow}^{\Gamma_6\Gamma_6}\left(\tfrac{1}{2}\tfrac{1}{2}0\right)$ and σ_i the Pauli spin matrices.

5. Zinc blendes with quasiatomic orbitals

Within ETB, a more common approach for the study of zinc blendes is the use of orbitals assigned to atomic positions[14,54–56] rather than Bravais lattice sites. This increases the spatial resolution and the size of the basis set.

The anion is assumed to have $\mathbf{d}_a = 0$, while the cation is at $\mathbf{d}_c = a(1,1,1)/4$. The blocks for the first-neighbor overlaps for VB states are then given by

$$E^{\Gamma_7^a\Gamma_7^c}\left(\tfrac{1}{4}\tfrac{1}{4}\tfrac{1}{4}\right) = \begin{pmatrix} E_{\uparrow\uparrow} & 0 \\ 0 & E_{\uparrow\uparrow} \end{pmatrix}, \tag{15}$$

$$E^{\Gamma_7^a\Gamma_8^c}\left(\tfrac{1}{4}\tfrac{1}{4}\tfrac{1}{4}\right) = \begin{pmatrix} \omega E_{\uparrow3} & 0 & -\omega^*\sqrt{3}E_{\uparrow3} & i\sqrt{2}E_{\uparrow3} \\ i\sqrt{2}E_{\uparrow3} & -\omega\sqrt{3}E_{\uparrow3} & 0 & \omega^*E_{\uparrow3} \end{pmatrix}, \tag{16}$$

$$E^{\Gamma_8^a\Gamma_7^c}\left(\tfrac{1}{4}\tfrac{1}{4}\tfrac{1}{4}\right) = \begin{pmatrix} \omega^*E_{3\uparrow} & -i\sqrt{2}E_{3\uparrow} \\ 0 & -\omega^*\sqrt{3}E_{3\uparrow} \\ -\omega\sqrt{3}E_{3\uparrow} & 0 \\ -i\sqrt{2}E_{3\uparrow} & \omega E_{3\uparrow} \end{pmatrix}, \tag{17}$$

and

$$E^{\Gamma_8^a\Gamma_8^c}\left(\tfrac{1}{4}\tfrac{1}{4}\tfrac{1}{4}\right) = \begin{pmatrix} E_{33} & -\omega^*[\sqrt{2}E_{3\bar{1}} + \sqrt{3}E_{3\bar{3}}] & iE_{3\bar{1}} & \omega E_{3\bar{3}} \\ -\omega[\sqrt{2}E_{3\bar{1}} + E_{3\bar{3}}/\sqrt{3}] & E_{33} & \omega^*E_{3\bar{3}} & iE_{3\bar{1}} + 2i\sqrt{2/3}E_{3\bar{3}} \\ -iE_{3\bar{1}} - 2i\sqrt{2/3}E_{3\bar{3}} & -\omega E_{3\bar{3}} & E_{33} & \omega^*[\sqrt{2}E_{3\bar{1}} + E_{3\bar{3}}/\sqrt{3}] \\ -\omega^*E_{3\bar{3}} & -iE_{3\bar{1}} & \omega[\sqrt{2}E_{3\bar{1}} + \sqrt{3}E_{3\bar{3}}] & E_{33} \end{pmatrix}, \tag{18}$$

and $E^{\Gamma_i^c\Gamma_j^a}\left(\tfrac{-1}{4}\tfrac{-1}{4}\tfrac{-1}{4}\right)$ can be obtained from

$$^{\alpha'\alpha}E_{i'i}^{\mu'\mu}(-\mathbf{R}_j - \mathbf{d}_{\alpha'} + \mathbf{d}_\alpha) = {}^{\alpha\alpha'}E_{i'i}^{\mu\mu'*}(\mathbf{R}_j + \mathbf{d}_{\alpha'} - \mathbf{d}_\alpha), \tag{19}$$

with $\alpha, \alpha' = a, c$ (anion or cation). The spinless model is recovered setting $E_{33} = E_{\uparrow\uparrow} = E_{xx}$, $E_{3\bar{1}} = E_{3\uparrow} = E_{\uparrow3} = E_{xy}/\sqrt{3}$ and $E_{3\bar{3}} = 0$. The nontrivial Hamiltonian matrix elements in the

bulk orbital representation are given in Table VIII.

C. Effective bond orbitals and k·p

We can obtain further insight into the nature of the LO's used as a basis set by noting that, for orbitals associated with the primitive cells (EBO's) and at $\mathbf{k}=0$, we have

TABLE VIII. Matrix elements for the zinc-blende structure (double group) for quasiatomic orbitals. The remaining matrix elements can be obtained from the Hermiticity of the Hamiltonian in the Bloch sum representation. The definitions $g_0 = 4(\cos\xi\cos\eta\cos\zeta - i\sin\xi\sin\eta\sin\zeta)$, $g_x = 4(-\cos\xi\sin\eta\sin\zeta + i\sin\xi\cos\eta\cos\zeta)$ (and cyclic permutations), are made, where $\xi \equiv k_x a/4$, $\eta \equiv k_y a/4$, and $\zeta \equiv k_z a/4$.

$H_{33}^{\Gamma_8^a \Gamma_8^c}(\mathbf{k})$	$E_{33}(\frac{1}{4}\frac{1}{4}\frac{1}{4})g_0$
$H_{33}^{\Gamma_8^a \Gamma_8^c}(\mathbf{k})$	$i[E_{3\bar{1}}(\frac{1}{4}\frac{1}{4}\frac{1}{4}) + \sqrt{3/2}E_{3\bar{3}}(\frac{1}{4}\frac{1}{4}\frac{1}{4})](g_x + ig_y)$
$H_{31}^{\Gamma_8^a \Gamma_8^c}(\mathbf{k})$	$iE_{3\bar{1}}(\frac{1}{4}\frac{1}{4}\frac{1}{4})g_z$
$H_{33}^{\Gamma_8^a \Gamma_8^c}(\mathbf{k})$	$iE_{3\bar{3}}(\frac{1}{4}\frac{1}{4}\frac{1}{4})(g_x - ig_y)/\sqrt{2}$
$H_{13}^{\Gamma_8^a \Gamma_8^c}(\mathbf{k})$	$-i[E_{3\bar{1}}(\frac{1}{4}\frac{1}{4}\frac{1}{4}) + \sqrt{1/6}E_{3\bar{3}}(\frac{1}{4}\frac{1}{4}\frac{1}{4})](g_x - ig_y)$
$H_{11}^{\Gamma_8^a \Gamma_8^c}(\mathbf{k})$	$E_{3\bar{3}}(\frac{1}{4}\frac{1}{4}\frac{1}{4})g_0$
$H_{11}^{\Gamma_8^a \Gamma_8^c}(\mathbf{k})$	$-iE_{3\bar{3}}(\frac{1}{4}\frac{1}{4}\frac{1}{4})(g_x + ig_y)/\sqrt{2}$
$H_{13}^{\Gamma_8^a \Gamma_8^c}(\mathbf{k})$	$i[E_{3\bar{1}}(\frac{1}{4}\frac{1}{4}\frac{1}{4}) + 2\sqrt{2/3}E_{3\bar{3}}(\frac{1}{4}\frac{1}{4}\frac{1}{4})]g_z$
$H_{\bar{i}j}^{\Gamma_8^a \Gamma_8^c}(k_x,k_y,k_z) = H_{ij}^{\Gamma_8^a \Gamma_8^c}(k_x,-k_y,-k_z)$	
$H_{\uparrow\uparrow}^{\Gamma_7^a \Gamma_7^c}(\mathbf{k})$	$E_{\uparrow\uparrow}(\frac{1}{4}\frac{1}{4}\frac{1}{4})g_0$
$H_{\uparrow\downarrow}^{\Gamma_7^a \Gamma_7^c}(\mathbf{k})$	0
$H_{\downarrow\downarrow}^{\Gamma_7^a \Gamma_7^c}(k_x,k_y,k_z) = H_{\uparrow\uparrow}^{\Gamma_7^a \Gamma_7^c}(k_x,-k_y,-k_z);$	
$H_{\downarrow\uparrow}^{\Gamma_7^a \Gamma_7^c}(k_x,k_y,k_z) = H_{\uparrow\downarrow}^{\Gamma_7^a \Gamma_7^c}(k_x,-k_y,-k_z)$	
$H_{3\uparrow}^{\Gamma_8^a \Gamma_7^c}(\mathbf{k})$	$-iE_{3\uparrow}(\frac{1}{4}\frac{1}{4}\frac{1}{4})(g_x + ig_y)/\sqrt{2}$
$H_{1\uparrow}^{\Gamma_8^a \Gamma_7^c}(\mathbf{k})$	0
$H_{1\uparrow}^{\Gamma_8^a \Gamma_7^c}(\mathbf{k})$	$-i\sqrt{3/2}E_{3\uparrow}(\frac{1}{4}\frac{1}{4}\frac{1}{4})(g_x - ig_y)$
$H_{3\uparrow}^{\Gamma_8^a \Gamma_7^c}(\mathbf{k})$	$-i\sqrt{2}E_{3\uparrow}(\frac{1}{4}\frac{1}{4}\frac{1}{4})g_z$
$H_{\bar{i}\downarrow}^{\Gamma_8^a \Gamma_7^c}(k_x,k_y,k_z) = -H_{i\uparrow}^{\Gamma_8^a \Gamma_7^c}(k_x,-k_y,-k_z)$	
$H_{\uparrow 3}^{\Gamma_7^a \Gamma_8^c}(\mathbf{k})$	$iE_{\uparrow 3}(\frac{1}{4}\frac{1}{4}\frac{1}{4})(g_x - ig_y)/\sqrt{2}$
$H_{\uparrow 1}^{\Gamma_7^a \Gamma_8^c}(\mathbf{k})$	0
$H_{\uparrow 1}^{\Gamma_7^a \Gamma_8^c}(\mathbf{k})$	$i\sqrt{3/2}E_{\uparrow 3}(\frac{1}{4}\frac{1}{4}\frac{1}{4})(g_x + ig_y)$
$H_{\uparrow 3}^{\Gamma_7^a \Gamma_8^c}(\mathbf{k})$	$i\sqrt{2}E_{\uparrow 3}(\frac{1}{4}\frac{1}{4}\frac{1}{4})g_z$
$H_{\downarrow\bar{i}}^{\Gamma_7^a \Gamma_8^c}(k_x,k_y,k_z) = -H_{\uparrow i}^{\Gamma_7^a \Gamma_8^c}(k_x,-k_y,-k_z)$	

$$H_{ii'}^{\mu\mu'}(\mathbf{k}=0) = \sum_{\mathbf{r}_j}\frac{1}{N(\mathbf{r}_j)}\sum_G D(G)_{is}^{\mu}E_{ss'}^{\mu\mu'}(\mathbf{r}_j)D(G^{-1})_{s'i'}^{\mu'}, \tag{20}$$

and by use of the orthogonality theorem for the irreducible representations[57] we arrive at

$$H_{ii'}^{\mu\mu'}(\mathbf{k}=0) = \delta_{\mu\mu'}\delta_{ii'}\sum_{\mathbf{r}_j,s}\frac{N(\mathcal{G}_0)}{N(\mathbf{r}_j)d^{\mu}}E_{ss'}^{\mu\mu'}(\mathbf{r}_j), \tag{21}$$

where $N(\mathcal{G}_0)$ is the number of operations of the point group and d^{μ} is the dimensionality of the μth irrep.

Thus, if one is constructing a model where there are no repeated irreps, we see that the Bloch sums of EBO's will exactly diagonalize the Hamiltonian at $\mathbf{k}=0$. In other words,

the Bloch sums of EBO's will be the zone-center solutions, making the connection between the EBO's and $\mathbf{k} \cdot \mathbf{p}$ basis evident.

IV. SUMMARY

In conclusion, we have constructed full-zone spin Hamiltonians for [001], [110], and [111] zinc-blende quantum wells. We then performed small-$\mathbf{k}_\parallel$ expansions of those Hamiltonians about the zone center, yielding their $\mathbf{k} \cdot \mathbf{p}$ counterparts. The $\mathbf{k} \cdot \mathbf{p}$ Hamiltonians thus obtained present spin-dependent terms that had not been previously described in the literature. In particular, we see that the Rashba Hamiltonian can be supplemented with third-order terms, which will need to be included in calculations where other sources of spin splitting are considered up to that order. We also generate additional, growth direction-dependent $\mathcal{O}(k_\parallel^3)$ contributions to the Dresselhaus Hamiltonian. These results hold for any system having the same symmetry as the studied quantum wells. The method we have employed is not restricted to these particular cases, as it extends the tight-binding formalism to include the treatment of spin by using double-group representations. This guarantees the systematic inclusion of all spin-related effects in the bands. Thus, our work can serve as the basis for numerical studies of large-scale nanostructures where spin effects are important, as well as an analytic tool for predicting spin properties in reduced-symmetry systems.

APPENDIX A: EMPIRICAL TIGHT-BINDING REVIEW

We review the empirical tight-binding method in order to set forth the notation employed in the paper. Following Ref. 14, we choose as our basis a collection of Löwdin-symmetrized orbitals[58] $|\phi_i^\mu;\mathbf{R}_j\rangle$, denoting an orbital centered on the lattice site $\mathbf{R}_j$ that transforms as the ith state of a basis set for the μth irrep of the point-group symmetry of the crystal (μ and i jointly define the band index of the state). Explicitly, they are given by

$$|\phi_i^\mu;\mathbf{R}_j\rangle = |\varphi_{i'}^{\mu'};\mathbf{R}_{j'}\rangle(S^{-1/2})_{i'i,\mathbf{R}_{j'}\mathbf{R}_j}^{\mu'\mu}, \tag{A1}$$

where $S^{-1/2}$ is the inverse of the square root of the overlap matrix S, with elements $S_{i'i,\mathbf{R}_{j'}\mathbf{R}_j}^{\mu'\mu} = \langle\varphi_{i'}^{\mu'};\mathbf{R}_{j'}|\varphi_i^\mu;\mathbf{R}_j\rangle$, and

$|\varphi_i^\mu; \mathbf{R}_j\rangle$ is the atomic orbital (or, in general, a state with finite overlap—e.g., a bond orbital) analogous to $|\phi_i^\mu; \mathbf{R}_j\rangle$. This is well defined, as the Löwdin symmetrization procedure ensures that the state will have the same symmetry properties as the underlying atomic orbital from which it is constructed.[14] As shown by Chang[33] and exploited in Sec. III, under certain conditions LO's provide the simplest connection to the $\mathbf{k} \cdot \mathbf{p}$ method. Another useful property is that LO's centered at different sites are orthogonal.

For the case of a bulk material, SK proceeded to construct bulk Bloch sums from the LO's:

$$|\phi_{i,\mathbf{k}}^\mu\rangle = \frac{1}{\sqrt{N}} \sum_{\mathbf{R}_j} e^{i\mathbf{k}\cdot\mathbf{R}_j} |\phi_i^\mu; \mathbf{R}_j\rangle, \qquad (A2)$$

where N is the number of lattice sites in the crystal and $\mathbf{k}$ lies within the first Brillouin zone. When the Schrödinger equation $H|\psi_\mathbf{k}\rangle = E|\psi_\mathbf{k}\rangle$ is expanded in terms of Bloch sums with coefficients $c_i^\mu(\mathbf{k}) \equiv \langle \phi_{i,\mathbf{k}}^\mu | \psi_\mathbf{k} \rangle$, it becomes an eigenvalue problem

$$\sum_{\mu',i'} \langle \phi_{i,\mathbf{k}}^\mu | H | \phi_{i',\mathbf{k}}^{\mu'} \rangle c_{i'}^{\mu'}(\mathbf{k}) = E_{i,\mathbf{k}}^\mu c_i^\mu(\mathbf{k}), \qquad (A3)$$

where $E_{i,\mathbf{k}}^\mu$ is the energy at point $\mathbf{k}$. The tight-binding matrix elements are easily seen to be given by

$$H_{ii'}^{\mu\mu'}(\mathbf{k}) \equiv \langle \phi_{i,\mathbf{k}}^\mu | H | \phi_{i',\mathbf{k}}^{\mu'} \rangle = \sum_{\mathbf{R}_j} e^{i\mathbf{k}\cdot\mathbf{R}_j} \langle \phi_i^\mu; \mathbf{0} | H | \phi_{i'}^{\mu'}; \mathbf{R}_j \rangle. \qquad (A4)$$

In ETB, the matrix elements on the right-hand side of Eq. (A4) are taken as adjustable parameters

$$E_{ii'}^{\mu\mu'}(\mathbf{R}_j) \equiv \langle \phi_i^\mu; \mathbf{0} | H | \phi_{i'}^{\mu'}; \mathbf{R}_j \rangle. \qquad (A5)$$

The sum over the neighboring sites in Eq. (A4) can be rewritten as

$$\langle \phi_{i,\mathbf{k}}^\mu | H | \phi_{i',\mathbf{k}}^{\mu'} \rangle = \sum_{\mathbf{r}_j} \frac{1}{N(\mathbf{r}_j)} \sum_G e^{i\mathbf{k}\cdot G\mathbf{r}_j} E_{ii'}^{\mu\mu'}(G\mathbf{r}_j), \qquad (A6)$$

where $\mathbf{r}_j$ is the collection of Bravais lattice sites not related by point-group ($\mathcal{G}_0$) operations G (i.e., sum over lattice points belonging to different stars) and $N(\mathbf{r}_j)$ is the number of operations that leave $\mathbf{r}_j$ invariant.

Since G acting on a state $|\phi_{i'}^{\mu'}; \mathbf{r}_j\rangle$ changes both the type of state and its lattice point, it is easy to see that $T_{G\mathbf{r}_j} = GT_{\mathbf{r}_j}G^{-1}$, where $T_{\mathbf{r}_j}$ translates a state $|\phi_{i'}^{\mu'}; \mathbf{0}\rangle$ into $|\phi_{i'}^{\mu'}; \mathbf{r}_j\rangle$. Thus, we have

$$E_{ii'}^{\mu\mu'}(G\mathbf{r}_j) = \langle \phi_i^\mu; \mathbf{0} | HT_{G\mathbf{r}_j} | \phi_{i'}^{\mu'}; \mathbf{0} \rangle = \langle \phi_i^\mu; \mathbf{0} | HGT_{\mathbf{r}_j}G^{-1} | \phi_{i'}^{\mu'}; \mathbf{0} \rangle. \qquad (A7)$$

Since $G \in \mathcal{G}_0$, we have that $HG = GH$; therefore, we arrive at

$$E_{ii'}^{\mu\mu'}(G\mathbf{r}_j) = D(G)_{is}^\mu E_{ss'}^{\mu\mu'}(\mathbf{r}_j) D(G^{-1})_{s'i'}^{\mu'}, \qquad (A8)$$

where we make use of

$$G|\phi_i^\mu; \mathbf{r}_j\rangle = |\phi_s^\mu; G\mathbf{r}_j\rangle D(G)_{si}^\mu \qquad (A9)$$

and $D(G)_{si}^\mu$ is the element for the matrix corresponding to operation G of the μth irrep of the crystal point group. We substitute Eq. (A8) into Eq. (A6) to obtain

$$H_{ii'}^{\mu\mu'}(\mathbf{k}) = \sum_{\mathbf{r}_j} \frac{1}{N(\mathbf{r}_j)} \sum_G e^{ik_t D(G)_{tt'}^{\mathrm{vec}} r_{j,t'}} D(G)_{is}^\mu E_{ss'}^{\mu\mu'}(\mathbf{r}_j) D(G^{-1})_{s'i'}^{\mu'}, \qquad (A10)$$

[Equation (1) in the text] where $D(G)^{\mathrm{vec}}$ is the representation of G for polar vectors, which in general will not be an irrep of the point group. This form allows for an easier computer implementation since there is no need to keep track of which neighbor positions have been visited and which not, and a single loop over all symmetry operations can be used.

SK present in their tables results for the Hamiltonian matrix elements computed with a method analogous to Eq. (A10), but only single-group irreps are used, which effectively does away with spin. In Sec. III we carry out calculations with double-group irreps, thus taking into account all spin effects within the single-particle approximation.

Note that this procedure can deal with general kinds of crystal lattices, not only those with a single atom per primitive cell, because any symmetry reduction due to the atom basis attached to each lattice site is mimicked by the imposed symmetry of the Löwdin orbitals. For example, in a zinc-blende structure orbitals transforming according to T_d (i.e., without definite parity) are attached to fcc lattice sites.

The inclusion of more than one type of orbital per primitive cell (i.e., the need to have orbitals attached to atomic sites rather than lattice sites) is easily achieved by introducing and extra index α for the atom type in the states and having $\mathbf{R}_j \to \mathbf{R}_j + \mathbf{d}_{\alpha'} - \mathbf{d}_\alpha$ in Eq. (A4), where $\mathbf{d}_\alpha$ is the offset of species α with respect to the lattice site. After that the derivation until Eqs. (A8) and (A10) continues unchanged.

APPENDIX B: SYMMETRY CONSIDERATIONS

It is useful to use all the available symmetries to reduce as much as possible the number of independent $E_{ss'}^{\mu\mu'}(\mathbf{r}_j)$'s. This becomes specially important when ETB is applied to lower dimensionality structures, as then the sum (A4) is not carried out for some directions (i.e., planar, linear or point orbitals are constructed).

1. Point-group symmetry

When a $\mathcal{G}_0$ operation G is such that $G\mathbf{r}_j = \mathbf{r}_j$ for a given $\mathbf{r}_j$, we obtain a number of consistency requirements for the neighbor matrix elements $E_{ii'}^{\mu\mu'}(\mathbf{r}_j)$ from Eq. (A8):

$$E_{ii'}^{\mu\mu'}(\mathbf{r}_j) = D(G)_{is}^\mu E_{ss'}^{\mu\mu'}(\mathbf{r}_j) D(G^{-1})_{s'i'}^{\mu'}. \qquad (B1)$$

2. Time reversal

For double-group irreps, the basis states can be labeled[39] by $i = -q_\mu, \ldots, -1/2, 1/2, \ldots, q_\mu$. For example, the top of the

valence band in zinc blendes would have $q_\mu = 3/2$, the bottom of the conduction band $q_\mu = 1/2$, etc. We employ the phase convention[39]

$$\Theta|\phi_i^\mu; \mathbf{r}_j\rangle \equiv |\tilde\phi_i^\mu; \mathbf{r}_j\rangle = (-1)^{q_\mu - i}|\phi_{-i}^\mu; \mathbf{r}_j\rangle \qquad \text{(B2)}$$

for the action of the time reversal operator Θ. Since Θ is antiunitary,[59] we will have

$$E_{ii'}^{\mu\mu'}(\mathbf{r}_j) = (-1)^{q_\mu + q_{\mu'}}(-1)^{i+i'} E_{-i,-i'}^{\mu\mu'*}(\mathbf{r}_j). \qquad \text{(B3)}$$

3. Rotation followed by translation

If there is an operation such that $G\mathbf{r}_j = -\mathbf{r}_j$, we can combine Eq. (A8) with the translational symmetry requirement $E_{ii'}^{\mu\mu'}(-\mathbf{r}_j) = E_{i'i}^{\mu'\mu*}(\mathbf{r}_j)$ to obtain

$$E_{i'i}^{\mu'\mu*}(\mathbf{r}_j) = D(G)_{is}^\mu E_{ss'}^{\mu\mu'}(\mathbf{r}_j) D(G^{-1})_{s'i'}^{\mu'}. \qquad \text{(B4)}$$

Now we can remove the complex conjugation operation by employing time reversal, Eq. (B3). The result is

$$E_{-i',-i}^{\mu'\mu}(\mathbf{r}_j) = (-1)^{q_\mu + q_{\mu'}}(-1)^{i+i'} D(G)_{is}^\mu E_{ss'}^{\mu\mu'}(\mathbf{r}_j) D(G^{-1})_{s'i'}^{\mu'}. \qquad \text{(B5)}$$

If the crystal has an inversion center, we will always be able to pick $G = I$, where I is the inversion operator. Then, since every irrep μ of a crystal with inversion will have a definite parity π_μ, we arrive at

$$E_{-i',-i}^{\mu'\mu}(\mathbf{r}_j) = (-1)^{q_\mu + q_{\mu'}}(-1)^{i+i'} \pi_\mu \pi_{\mu'} E_{ii'}^{\mu\mu'}(\mathbf{r}_j). \qquad \text{(B6)}$$

4. Bloch sums

It is also convenient to state explicitly the transformation properties of Bloch sums and their matrix elements. This can reduce the number of elements that need to be specified.

Combining Eqs. (A1) and (A9) it is easy to see that

$$G|\phi_{i,\mathbf{k}}^\mu\rangle = |\phi_{s,G\mathbf{k}}^\mu\rangle D(G)_{si}^\mu, \qquad \text{(B7)}$$

which leads to the relationship[36]

$$H_{ii'}^{\mu\mu'}(\mathbf{k}) = D(G)_{is}^\mu H_{ss'}^{\mu\mu'}(G^{-1}\mathbf{k}) D(G^{-1})_{s'i'}^{\mu'}, \qquad \text{(B8)}$$

constraining the values of the Hamiltonian matrix elements between Bloch sums.

APPENDIX C: MODELS WITH A FINITE NUMBER OF BANDS

The procedure described in Appendix A will only yield the exact Hamiltonian when an infinite number of LO's is included and interaction with all neighbors is accounted for. Of course, the localized character of the LO's will limit the neighbor distance at which there is non-negligible overlap. On the other hand, since the number of included neighbors is directly related to the number of Fourier components of the bands, the effect of coupling to bands outside the model—which will add to the number of Fourier components—can be modeled by increasing the range of the effective Hamiltonian interaction.[60]

In the extreme case where only two bands are included (say, spin up and spin down), a large number of included neighbors will provide a good description of the bands. In this context Kramers degeneracy is easily shown for doubly degenerate irreps (i.e., doubly degenerate at the zone center, but not *a priori* at a general $\mathbf{k}$ point). Labeling $\mu \to 2q_\mu$, time reversal combined with inversion symmetry [Eq. (B6)] implies $E_{\uparrow\uparrow}^{11}(\mathbf{r}_j) = E_{\downarrow\downarrow}^{11}(\mathbf{r}_j)$ and $E_{\uparrow\downarrow}^{11}(\mathbf{r}_j) = E_{\downarrow\uparrow}^{11}(\mathbf{r}_j) = 0$. Thus, the spin 2×2 Hamiltonian takes on the form

$$H_{\text{inv}}^{11} = \begin{pmatrix} H_{\uparrow\uparrow}(\mathbf{k}) & 0 \\ 0 & H_{\uparrow\uparrow}(\mathbf{k}) \end{pmatrix}, \qquad \text{(C1)}$$

which shows that the bands will indeed be degenerate at a general $\mathbf{k}$ point.

*Electronic address: Xavier.Cartoixa@uab.es

[1] G. A. Prinz, Phys. Today **48**(4), 58 (1995).

[2] S. A. Wolf, D. D. Awschalom, R. A. Buhrman, J. M. Daughton, S. von Molnár, M. L. Roukes, A. Y. Chtchelkanova, and D. M. Treger, Science **294**, 1488 (2001).

[3] G. Dresselhaus, Phys. Rev. **100**, 580 (1955).

[4] Y. A. Bychkov and E. I. Rashba, J. Phys. C **17**, 6039 (1984).

[5] M. I. D'yakonov and V. I. Perel', Fiz. Tverd. Tel. **13**, 3581 (1971) [Sov. Phys. Solid State **13**, 3023 (1972)].

[6] M. I. D'yakonov and V. Y. Kachorovskiǐ, Fiz. Tekh. Poluprovodn. **20**, 178 (1986) [Sov. Phys. Semicond. **20**, 110 (1986)].

[7] N. S. Averkiev and L. E. Golub, Phys. Rev. B **60**, 15582 (1999).

[8] A. Voskoboynikov, S. S. Lin, C. P. Lee, and O. Tretyak, J. Appl. Phys. **87**, 387 (2000).

[9] D. Z.-Y. Ting and X. Cartoixà, Appl. Phys. Lett. **81**, 4198 (2002).

[10] T. Koga, J. Nitta, H. Takayanagi, and S. Datta, Phys. Rev. Lett. **88**, 126601 (2002).

[11] X. Cartoixà, D. Z.-Y. Ting, and Y.-C. Chang, Appl. Phys. Lett. **83**, 1462 (2003).

[12] J. Schliemann, J. C. Egues, and D. Loss, Phys. Rev. Lett. **90**, 146801 (2003).

[13] X. Cartoixà, D. Z.-Y. Ting, and Y.-C. Chang, Phys. Rev. B **71**, 045313 (2005).

[14] J. C. Slater and G. F. Koster, Phys. Rev. **94**, 1498 (1954).

[15] F. Oyafuso, G. Klimeck, R. C. Bowen, T. Boykin, and P. von Allmen, Phys. Status Solidi C **4**, 1149 (2003).

[16] N. Hamada, S. I. Sawada, and A. Oshiyama, Phys. Rev. Lett. **68**, 1579 (1992).

[17] D. J. Chadi, Phys. Rev. B **16**, 790 (1977).

[18] T. B. Boykin, Phys. Rev. B **57**, 1620 (1998).

[19] J. Luo, H. Munekata, F. F. Fang, and P. J. Stiles, Phys. Rev. B **38**, 10142 (1988).

[20] J. Luo, H. Munekata, F. F. Fang, and P. J. Stiles, Phys. Rev. B **41**, 7685 (1990).

[21] T. Schäpers, G. Engels, J. Lange, T. Klocke, M. Hollfelder, and H. Lüth, J. Appl. Phys. **83**, 4324 (1998).

[22] O. Krupin, G. Bihlmayer, K. Starke, S. Gorovikov, J. E. Prieto, K. Dobrich, S. Blugel, and G. Kaindl, Phys. Rev. B **71**, 201403(R) (2005).

[23] D. Popovic, F. Reinert, S. Hufner, V. G. Grigoryan, M. Springborg, H. Cercellier, Y. Fagot-Revurat, B. Kierren, and D. Malterre, Phys. Rev. B **72**, 045419 (2005).

[24] H. Cercellier, Y. Fagot-Revurat, B. Kierren, F. Reinert, D. Popovic, and D. Malterre, Phys. Rev. B **70**, 193412 (2004).

[25] J. Henk, M. Hoesch, J. Osterwalder, A. Ernst, and P. Bruno, J. Phys.: Condens. Matter **16**, 7581 (2004).

[26] Y. M. Koroteev, G. Bihlmayer, J. E. Gayone, E. V. Chulkov, S. Blugel, P. M. Echenique, and P. Hofmann, Phys. Rev. Lett. **93**, 046403 (2004).

[27] M. Hoesch, M. Muntwiler, V. N. Petrov, M. Hengsberger, L. Patthey, M. Shi, M. Falub, T. Greber, and J. Osterwalder, Phys. Rev. B **69**, 241401(R) (2004).

[28] F. Reinert, J. Phys.: Condens. Matter **15**, S693 (2003).

[29] G. Nicolay, F. Reinert, S. Hufner, and P. Blaha, Phys. Rev. B **65**, 033407 (2002).

[30] E. Rotenberg, J. W. Chung, and S. D. Kevan, Phys. Rev. Lett. **82**, 4066 (1999).

[31] T. C. Shen, J. Y. Ji, M. A. Zudov, R. R. Du, J. S. Kline, and J. R. Tucker, Appl. Phys. Lett. **80**, 1580 (2002).

[32] W. H. Lau and M. E. Flatte, Phys. Rev. B **72**, 161311(R) (2005).

[33] Y. C. Chang, Phys. Rev. B **37**, 8215 (1988).

[34] G. T. Einevoll and Y. C. Chang, Phys. Rev. B **40**, 9683 (1989).

[35] L. M. Falicov, *Group Theory and Its Physical Applications*, 1st ed., Chicago Lectures in Physics (The University of Chicago Press, Chicago, 1966).

[36] G. L. Bir and G. E. Pikus, *Symmetry and Strain-Induced Effects in Semiconductors*, 1st ed. (Wiley, New York, 1974).

[37] K. Shirai, http://library.wolfram.com/infocenter/MathSource/4634/.

[38] Y. Onodera and M. Okazaki, J. Phys. Soc. Jpn. **21**, 2400 (1966).

[39] G. F. Koster, J. O. Dimmock, R. G. Wheeler, and H. Statz, *Properties of the Thirty-Two Point Groups*, 1st ed. (MIT Press, Cambridge, MA, 1963).

[40] K. C. Hass, H. Ehrenreich, and B. Velicky, Phys. Rev. B **27**, 1088 (1983).

[41] X. Cartoixà, D. Z.-Y. Ting, and T. C. McGill, Phys. Rev. B **68**, 235319 (2003).

[42] L. Vervoort, R. Ferreira, and P. Voisin, Semicond. Sci. Technol. **14**, 227 (1999).

[43] R. Eppenga and M. F. H. Schuurmans, Phys. Rev. B **37**, 10923 (1988).

[44] E. A. de Andrada e Silva, Phys. Rev. B **46**, R1921 (1992).

[45] The derivation of the last term in (3) from bulk properties requires constructing the bulk spin Hamiltonian to $\mathcal{O}(k^5)$ and only then replacing $\hat{k}_z^{2n} \rightarrow \langle \hat{k}_z^{2n} \rangle$.

[46] X. Cartoixà, D. Z.-Y. Ting, and T. C. McGill, Nanotechnology **14**, 308 (2003).

[47] Y. Ohno, R. Terauchi, T. Adachi, F. Matsukura, and H. Ohno, Phys. Rev. Lett. **83**, 4196 (1999).

[48] Y. E. Kitaev, A. G. Panfilov, P. Tronc, and R. A. Evarestov, J. Phys.: Condens. Matter **9**, 277 (1997).

[49] E. O. Kane, in *Semiconductors and Semimetals*, edited by R. K. Willardson and A. C. Beer (Academic, New York, 1966), Vol. 1, pp. 75–100.

[50] J.-M. Jancu, R. Scholz, E. A. de Andrada e Silva, and G. C. LaRocca, Phys. Rev. B **72**, 193201 (2005).

[51] M. Cardona, N. E. Christensen, and G. Fasol, Phys. Rev. B **38**, 1806 (1988).

[52] P. C. Mathur and S. Jain, Phys. Rev. B **19**, 3152 (1979).

[53] M. W. Heller and R. G. Hamerly, J. Appl. Phys. **57**, 4626 (1985).

[54] D. J. Chadi and M. L. Cohen, Phys. Status Solidi B **68**, 405 (1975).

[55] W. A. Harrison, *Electronic Structure and the Properties of Solids*, 1st ed. (Dover, Mineola, NY, 1989).

[56] P. Vogl, H. P. Hjalmarson, and J. D. Dow, J. Phys. Chem. Solids **44**, 365 (1983).

[57] W.-K. Tung, *Group Theory in Physics*, 1st ed. (World Scientific, Singapore, 1985).

[58] P.-O. Löwdin, J. Chem. Phys. **18**, 365 (1950).

[59] J. J. Sakurai, *Modern Quantum Mechanics*, 1st ed. (Addison-Wesley, Redwood City, CA, 1985).

[60] D. Z.-Y. Ting and Y.-C. Chang, Phys. Rev. B **36**, 4359 (1987).